

Temporal-mode detector tomography of a quantum pulse gate

Vahid Ansari,^{1,*} Georg Harder,¹ Markus Allgaier,¹ Benjamin Brecht,^{1,2} and Christine Silberhorn¹

¹*Integrated Quantum Optics, Paderborn University,
Warburger Strasse 100, 33098 Paderborn, Germany*

²*Clarendon Laboratory, Department of Physics, University of Oxford, Parks Road, OX1 3PU, United Kingdom*

Encoding information in temporal modes (TMs) is an intriguing scheme in quantum information science. The main practical challenge, however, is to design a device that operates on phase and amplitude of TMs carried by quantum states. The quantum pulse gate (QPG) is a mode selective sum-frequency generation designed for this task. Here, we perform a full modal characterisation of a QPG detector using weak coherent input states in well-defined TMs. We reconstruct a full set of measurement operators, which show an average fidelity of 85% to a theoretically ideal device when operating on a 7-dimensional space. Then we take the characterised measurement operators of the QPG to calibrate the device. Using the calibrated device, we show that QPG can perform TM state tomography with fidelities of 99%.

INTRODUCTION

The temporal or spectral shape of light is an important resource in many classical applications such as signal multiplexing in communications. Harnessing this degree of freedom for quantum states will affect an equally broad range of applications: high-dimensional quantum communication [1], realisation of deterministic quantum gates [2], interfacing photons and material systems [3, 4] and enhanced-resolution spectroscopy [5]. All these applications require the capability of shaping quantum states, e.g. single photons, into specific temporal modes (TMs), defined by the amplitude and phase of the electric field, and to measure them in a TM-resolved manner. The operations need to work with high quantum efficiency and on superpositions of TMs, i.e. preserve phase of TMs. Frequency conversion allows us to perform these manipulations as it can be understood as a set of frequency beamsplitters converting input TMs to different output TMs. In particular, if the conversion process is a single-mode process in the sense that it converts exactly one controllable TM input mode to one TM output mode, we call it a quantum pulse gate (QPG) [6–11]. A QPG can be constructed, for example, with a waveguide built from a tailored nonlinear material and a shaped strong pump pulse. Such a process can be used to shape TM-states, interfere states in different TMs and detect TM-states selectively. In this publication we focus on the latter application, i.e. the QPG as a TM detector. We characterise the modal performance of the device by shaping a tomographically complete set of input states. The shaping can be performed with very high accuracy using a commercial pulse shaper and weak coherent states. This characterises the process, including all the modal imperfections, and allows us to compare the expected behaviour to the actual experimental behaviour. Furthermore, it allows us to significantly increase the fidelities of TM-state tomography.

In a recent publication, Manurkar et al [11] demonstrated a QPG in with reasonably high selectivities for

certain TMs with high conversion efficiencies. However, they do not fully characterise the operation on the chosen Hilbert space. Such characterisation is the main focus of this work. In comparison to Manurkar et al, we stay at a low conversion efficiency of a few percent to avoid a change of the modal properties due to the time-ordering effects [8, 12–15]. Increasing the efficiency by increasing either the power of the pump pulse or the length of the nonlinear interaction generally drives the process from single-mode to multimode. While the accompanied mode distortions can be compensated by experimentally optimising the TMs of the pump and input fields, the multimodeness cannot be avoided. One proposed solution to this problem is to use two consecutive crystals with 50% conversion efficiency for each [16, 17]. The difficulty then is that the pulses have to be temporally shifted back to their initial relative positions between the crystals. Nevertheless, this approach seems to be the most promising route towards unit conversion efficiency and single-mode operation.

FREQUENCY CONVERSION AND MODE SELECTIVE MEASUREMENTS

We express our states in terms of broadband temporal modes (TMs)

$$\hat{A}_i = \int f_i(\omega) \hat{a}(\omega) d\omega, \quad (1)$$

where $f_i(\omega)$ are frequency amplitudes and $\hat{a}(\omega)$ the annihilation operators for the central frequency ω . The spectral intensity $|f_i(\omega)|^2$, can be measured with a standard spectrometer. In the following, the modes \hat{A}_i form our discrete basis of dimension d , i.e. the functions $f_i(\omega)$ are orthonormal and $0 \leq i < d$. In the experiment, we take $d = \{5, 7\}$ and $f_i(\omega)$ as Hermite-Gaussian functions of order i .

Before giving the sketch of the TM tomography, we briefly review the formalism of QPG as a mode-selective

frequency conversion (FC). FC in general is a beam splitter acting on TMs, which has a Hamiltonian $\hat{H}_{\text{FC}} = \theta \iint f(\omega_{\text{out}}, \omega_{\text{in}}) \hat{b}^\dagger(\omega_{\text{out}}) \hat{a}(\omega_{\text{in}}) d\omega_{\text{in}} d\omega_{\text{out}} + \text{h.c.}$, where \hat{a} and \hat{b} are the annihilation operators for the two beam-splitter modes. The transfer function

$$f^\alpha(\omega_{\text{out}}, \omega_{\text{in}}) = \alpha(\omega_{\text{pump}}) \Phi(\omega_{\text{in}}, \omega_{\text{out}}) \quad (2)$$

is given by the pump amplitude $\alpha(\omega_{\text{pump}})$ and the phase-matching function $\Phi(\omega_{\text{in}}, \omega_{\text{out}})$ of the crystal [6, 7]. From here we use an index α to indicate that we can adjust the process by shaping the pump spectrum. Using the Schmidt decomposition, the transfer function $f^\alpha(\omega_{\text{out}}, \omega_{\text{in}})$ can be decomposed into its eigenmodes defining new TM operators \hat{C}_k^α and \hat{D}_k^α , thus reducing the integral to the following sum

$$\hat{H}_{\text{FC}}^\alpha = \theta \sum_k \lambda_k^\alpha (\hat{D}_k^\alpha)^\dagger \hat{C}_k^\alpha + \text{h.c.}, \quad (3)$$

where λ_k^α are the eigenvalues of the decomposition, normalised as $\sum_k |\lambda_k^\alpha|^2 = 1$, and θ is the gain of the process. The orthogonality of the eigenmodes ensures that we can regard the FC as independent beam splitters with a reflectivity or conversion efficiency of $\eta_k^\alpha = \sin^2(|\theta \lambda_k^\alpha|)$. As sketched in Fig. 1, we have no input in mode D and measure the mean photon number of the converted light, which is

$$n = \sum_k \eta_k^\alpha \langle (\hat{C}_k^\alpha)^\dagger \hat{C}_k^\alpha \rangle. \quad (4)$$

To calculate what this means for a given input spectral shape, we decompose the mode β of the input state into the eigenmodes of the FC

$$\beta = \sum_k v_k^{\alpha\beta} \hat{C}_k^\alpha. \quad (5)$$

Then we can rewrite the mean photon number as

$$n^{\alpha\beta} = N^\beta \sum_k \eta_k^\alpha |v_k^{\alpha\beta}|^2, \quad (6)$$

where N^β is the total mean photon number of the input state and $|v_k^{\alpha\beta}|^2$ the overlap between the input mode β and the k -th eigenmode of the conversion process for a pump setting α . Interestingly, this is valid for all photon number distributions including the coherent states we use here.

We can also rewrite this in vector notation as

$$n^{\alpha\beta} = N^\beta \sum_k \eta_k^\alpha |\langle \beta | k^\alpha \rangle|^2 \quad (7)$$

$$= \langle \beta | \hat{M}^\alpha | \beta \rangle, \quad (8)$$

where $\hat{M}^\alpha = \sum_k \eta_k^\alpha |k^\alpha\rangle \langle k^\alpha| = \sum_{ij} m_{ij}^\alpha |i\rangle \langle j|$ is our measurement operator, $|i\rangle$ the TM basis from Eq. 1, $|\beta\rangle$ the input state and $|k^\alpha\rangle$ the eigenvectors of the process. The

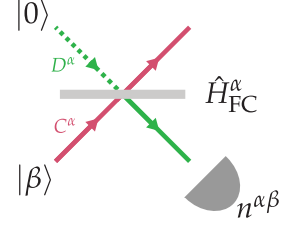


FIG. 1. Outline of QPG operation. The QPG is a beam-splitter operating on a TM defined by the index α . For the detector tomography, we send coherent states $|\beta\rangle$ to the QPG and at the converted (reflected) port we measure the number of converted photons using a bucket detector, noted as $n^{\alpha\beta}$.

idea of detector tomography is to probe the matrix \hat{M}^α with different states $|\beta\rangle$. All we have to do is to generate a tomographically complete set of probe states and employ standard detector tomography with the measured mean photon numbers for each setting, thus determining the elements m_{ij}^α . Diagonalising this matrix, we get the FC eigenmodes $|k^\alpha\rangle$ and efficiencies η_k^α . This fully characterises the input-mode structure of the FC. An ideal QPG has only one eigenmode, i.e. \hat{M}^α has only one non-zero eigenvalue, and the shape of the eigenmode would reflect the shape of the pump $k_0^\alpha(\omega) = \alpha(-\omega)$.

It is worth noting that while the number of modes of the FC is in principle infinite, the probe space is only finite dimensional. Despite this, the reconstruction of the FC within the probe space is accurate. A simple example is when the TMs of the pump and input are not perfectly matched, e.g. in their central frequencies. This can change the overall conversion efficiency $\text{tr}(\hat{M}^\alpha) = \sum_k \eta_k^\alpha$ for different pump shapes α . We therefore try to match the central frequencies and bandwidths of the input and pump TMs to cover as much of the FC space as possible.

EXPERIMENT

The type-II sum-frequency process happens in a 17 mm LiNbO₃ crystal with Ti indiffused waveguides and a poling period of 4.4 μm . The waveguides are designed to be spatially single mode at 1550 nm. The outline of the experimental setup is sketched in Fig. 2. We take ultrashort pulses from a Ti:sapphire oscillator to pump an optical parametric oscillator (OPO). With this configuration we have Gaussian pulses at central wavelengths of 873 nm and 1550 nm, for the pump and signal fields respectively, with amplitude FWHM of 3.35 THz for both fields. We use a home-built pulse shaper to shape the pump and a commercial pulse shaper (Finisar waveshaper 4000) to shape the input light pulses, with resolutions of 22 pm and 8 pm respectively. Both pulse shapers use a reflective liquid crystal on silicon spatial

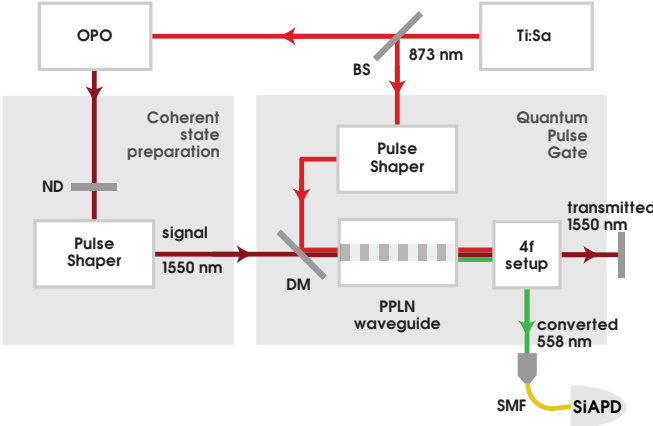


FIG. 2. Experimental setup. A femtosecond titanium:sapphire (Ti:Sa) oscillator with repetition rate of 80 MHz is used to pump an optical parametric oscillator (OPO). The pump of the QPG is obtained from a tap-off of Ti:Sa laser. The input signal field is prepared by attenuating the OPO output to a mean photon number of less than a photon per pulse by using neutral density (ND) filters. We use SLMs in a folded 4f-setup to shape the desired spectral amplitude and phase for the both fields. Then pump and input fields are combined on a dichroic mirror (DM) and coupled to a home-built periodically poled lithium niobate (PPLN) waveguide, held at 207°C. After the PPLN waveguide, the up-converted photons with a green colour are selected by a 4f-setup and coupled to a silicon avalanche photodiode (SiAPD), through a single-mode fibre (SMF).

light modulator (LCoS-SLM) in the Fourier plane of a folded 4f setup. We used spectral interferometry to optimise both pulse shapers to be dispersion free. The shaping resolutions are better than the resolution we require in this experiment. For example, while we could prepare the 20th-order Hermite-Gaussian mode, we only use the first 7 modes as our basis. For the tomography, we choose a bandwidth of 0.4 THz (FWHM of the amplitude of the Gaussian mode) for both fields.

Can you also add vendors and part numbers/names of the components?

The key property of a QPG is the group-velocity matching (GVM) between input and pump. In Fig. 3 we plot the intensity of the phasematching function $|\Phi(\lambda_{\text{in}}, \lambda_{\text{out}})|^2$, measured with a scanning continuous wave input and adjusted pump pulses on a high-resolution spectrograph. A perfect GVM condition results in the zero gradient of phasematching function. The marginal spectrum of this function, plotted on the left side in Fig. 3, shows an asymmetric structure with decaying side lobes. This can be explained by an inhomogeneity of the effective refractive index along the waveguide, equivalent to a variation of the poling period. A quadratic variation of the poling period can introduce such asymmetric side peaks. In the experiment, we also have a 4f setup on the SFG line that allows us to filter

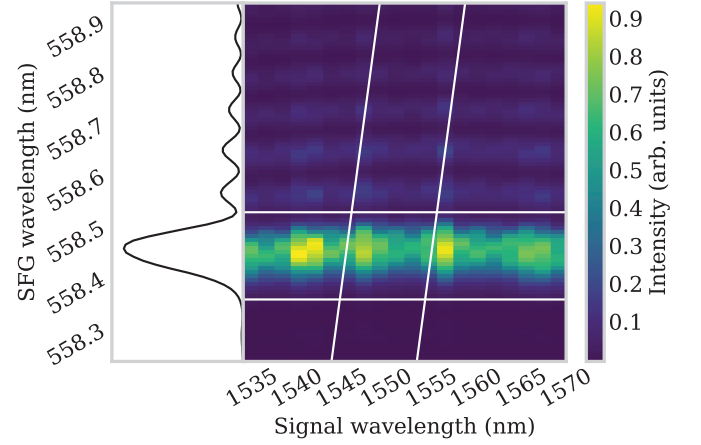


FIG. 3. Phasematching function of the QPG. Right: The zero gradient of the phasematching function $\Phi(\omega_{\text{in}}, \omega_{\text{out}})$, is an indicator of group-velocity matching between input signal and the pump field. The diagonal white lines are marking the orientation of the pump amplitude $\alpha(\omega_{\text{in}} + \omega_{\text{out}})$ and the bandwidth we use in this paper. The horizontal white lines are showing the bandwidth of the 4f-setup used to filter the SFG signal. Left: marginal distribution of the plot on the right side. Asymmetries are due to inhomogeneity of the effective refractive index along the waveguide.

out these side lobes.

One common complication with waveguides is that different spatial mode combinations have different phase-matchings. In our case, these do not overlap with the phasematching for the fundamental mode shown in Fig. 3 and we can simply filter them out spectrally. Nevertheless, special care is taken to optimise the coupling of both beams into the waveguide for the desired process and minimise the intensity in higher order modes.

We shape both the pump and the input according to mutually unbiased bases (MUBs) [18]. These have the property that for a dimension d , there are $(d + 1)$ bases such that overlaps between states from different bases are always $1/d$, hence unbiased. This ensures that the space is uniformly probed. Furthermore, the total set is overcomplete, helping to reduce systematic experimental errors. Since for each pump shape, we have to run the full characterisation with $(d + 1)d$ input modes, the total number of measurements for $d = 5$ and $d = 7$ are 900 and 3136, respectively. For each of them, we record counts for about 1 s at count rates up to 10^5 counts/s. Since the count rates are directly proportional to the powers of the pump and the input, we record both values after the waveguide and normalise the count rates accordingly to account for small drifts in the setup (of the order of 10%).

TABLE I. Purities and fidelities of QPG measurement operators, expressed in percent.

d	5 (unfiltered)	5	7
$\mathcal{P}_{\text{measured}}$	71.9 ± 6.4	92.0 ± 2.4	81.1 ± 3.5
$\mathcal{F}_{\text{measured}}$	77.8 ± 8.6	91.2 ± 4.6	84.7 ± 4.2
$\mathcal{P}_{\text{theory}}$		93.9 ± 2.6	90.9 ± 3.5
$\mathcal{F}_{\text{theory}}$		97.9 ± 0.8	97.1 ± 1.0

RESULTS

To find the measurement operators \hat{M}^α from the data we perform a weighted least squares fit

$$\min_{\hat{M}^\alpha} \sum_{\beta} \frac{|f^{\alpha\beta} - \langle \beta | \hat{M}^\alpha | \beta \rangle|^2}{f^{\alpha\beta}}, \quad (9)$$

where $f^{\alpha\beta}$ are normalised count rates and \hat{M}^α is constrained to be Hermitian and positive semidefinite. Since each setting α is an independent measurement, we do not put a constraint on the sum of operators. In Fig. 4 we show the first eigenmodes of all measurement operators for 7 dimensions. They closely resemble the ideal MUB states. To quantify how accurate the results are, we calculate the purities $\mathcal{P}^\alpha = \text{tr}([\hat{M}^\alpha]^2)/\text{tr}(\hat{M}^\alpha)^2$ and the fidelities $\mathcal{F}^\alpha = \sqrt{\langle \alpha | \hat{M}^\alpha | \alpha \rangle / \text{tr}(\hat{M}^\alpha)}$ with the ideal operators $|\alpha\rangle\langle\alpha|$. We perform the characterisation in 5 and 7 dimensions, whereas for 5 dimensions we also compare the two experimental settings with and without a spectral filter in the output mode. As mentioned above, the spectral filter blocks the side peaks of the phasematching. The average values with their respective standard deviations are shown in Table I.

For comparison we also show theoretical values assuming a Gaussian horizontal phasematching and perfect pump shaping. The imperfections in this case originate from the fact that the phasematching is only about five times narrower than the pump, leading to small correlations in the transfer function. This also explains why suppressing the side lobes of the output spectrum improves the purity from 72% to 92%. A comparison of the eigenmodes for these two cases shows that the first eigenmode hardly changes. Thus the spectral filtering suppresses the higher order spectral modes introduced by the side lobes of the phasematching, or in other words drives the QPG to single-modeness. Going from 5 to 7 dimensions slightly lowers both the purities and the fidelities. One reason is that the fine structures of the pump at higher dimensions, again, can introduce some correlations which also reduce the theoretical values. However, the expected reduction is much smaller than what we measure. Imperfections in the pulse shaping are also a greater problem for higher dimensions. Since with the increase of dimensionality the total bandwidth both in time and frequency

increases, the relative phases and amplitudes have to be accurate over a broader range in both time and frequency. Furthermore, the measurement time increases drastically which makes the experiment more susceptible to drifts in the setup. With the current experimental setup, the 7-dimensional characterisation takes about 2 hours.

The overall high fidelities we measure in this work demonstrates that the QPG can operate on arbitrary TMs in a selective way. The fidelities also quantify the mode selectivity since the normalised conversion efficiency is given by \mathcal{F}^2 . In the 5-dimensional case, that means that the desired mode gets converted with 83% efficiency and any orthogonal mode gets converted with less than 17%. However, with the measurement operators we have much more information than just the mode selectivity. For a task like state tomography, a perfect QPG is not required. All we need is mode-sensitivity and the knowledge of our mode detector, which we have with the matrices \hat{M}^α .

In the following we investigate the performance of the QPG for state tomography. For this purpose, we prepare states like $\hat{\rho} = |\beta\rangle\langle\beta|$, which are different from the characterisation set we use for the detector tomography. To ensure fair benchmarking we prepare twenty different input states where half of them are generated randomly. Then we use the $(d+1)d$ QPG settings α to reconstruct the input state. We measure the normalised probabilities f^α and minimise

$$\min_{\hat{\rho}} \sum_{\alpha} \frac{|f^\alpha - \text{tr}(\hat{\rho}\hat{M}^\alpha)|^2}{f^\alpha}, \quad (10)$$

under the constraints that $\hat{\rho}$ is Hermitian, positive semidefinite and $\text{tr}(\hat{\rho}) = 1$. First, we assume a perfect QPG with ideal measurement operators and reconstruct the input states. Since the prepared inputs are coherent states in well-defined TMs, we expect to reconstruct pure states. The average fidelities and their standard deviations measured for all input states are listed in Table II, which shows a modest fidelity of the state tomography. This is because the slight multimodeness of the QPG operation translates into the mixedness of the reconstructed states and leads to inaccurate tomography. It is also expected, considering the phasematching function in Fig. 3, that as the dimension increases the degree of multimodeness of QPG also grows. To understand how the number of present modes in the operation of QPG affects the purity of reconstructed states, in Fig. 5 we plot the purity of numerically modelled QPG (defined as $1/\sum_k \lambda_k^2$) up to dimension of 32. To examine the scalability of a QPG as a TM selective device, we also modelled the purity of the QPG presented in [11]. The higher purity of our QPG is owed to the narrow linewidth of phasematching and the tailored GVM condition of the nonlinear waveguide. These features lead to a frequency decorrelation of the transfer function defined by the phasematching and

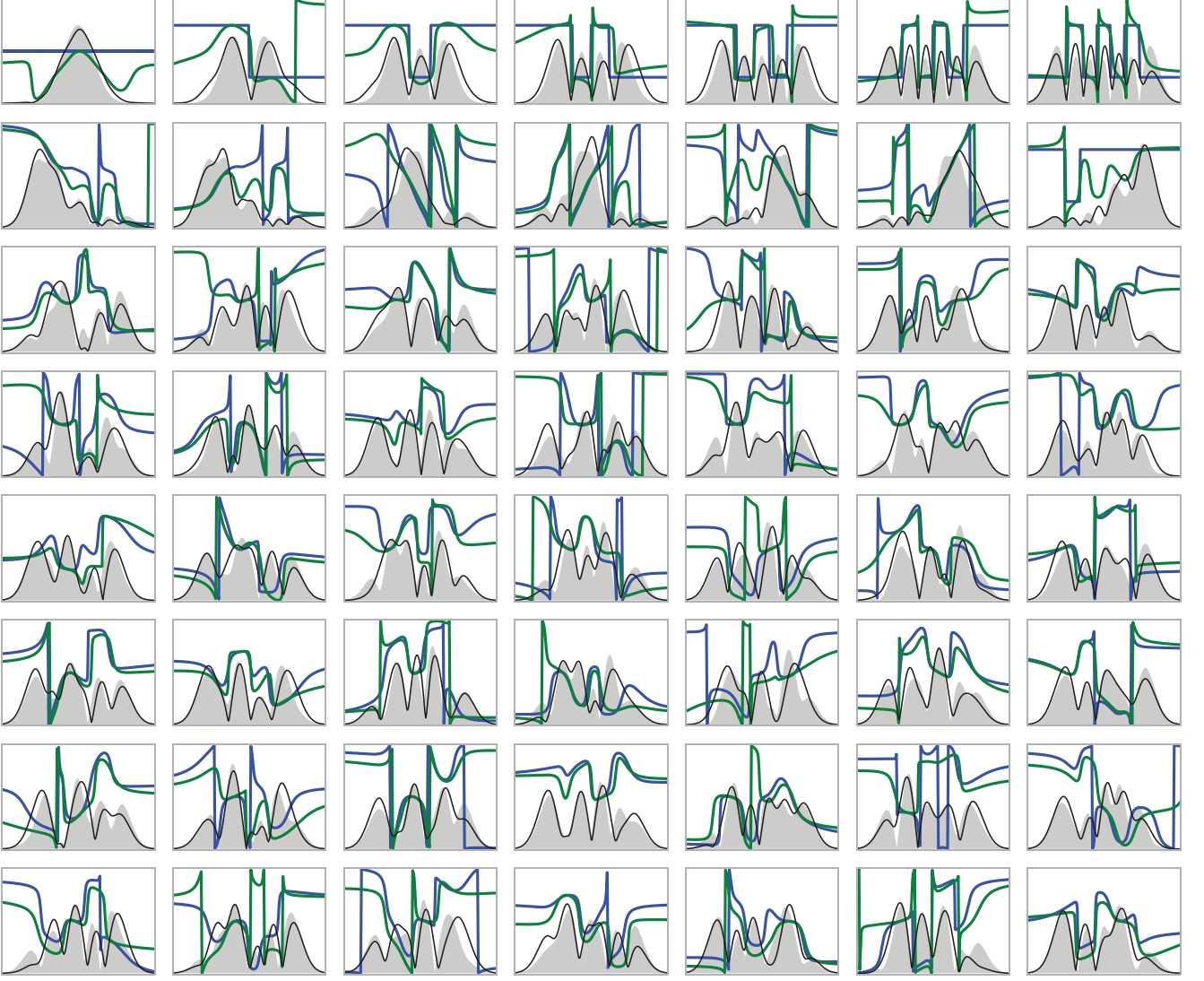


FIG. 4. The first eigenvectors of the 7x6 measurement operators. For each plot, the x-axis corresponds to the frequency and the y-axis to the amplitude and phase. Black and green lines are the measured amplitudes and phases, respectively; shaded areas and blue lines are theoretical MUB states. Note that the phase is 2π periodic, which is also the interval of the y-axis. A π phase-jump thus corresponds to half the y-range. Note also that phases are only meaningful when there is significant amplitude present.

TABLE II. Purities and fidelities of state tomography, expressed in percent.

	d 5 (unfiltered)	5	7
\mathcal{P}	68.0 ± 7.9	75.3 ± 9.8	61.9 ± 5.2
\mathcal{F}	74.2 ± 12.6	87.9 ± 4.1	81.3 ± 3.1

TABLE III. Purities and fidelities of state tomography with calibrated QPG, expressed in percent.

	d 5 (unfiltered)	5	7
\mathcal{P}	93.1 ± 3.8	97.2 ± 1.6	95.7 ± 1.7
\mathcal{F}	97.1 ± 1.5	99.1 ± 0.5	98.8 ± 0.4

pump, as seen in Fig. 3.

To improve the quality of the state tomography we can use the characterised measurement operators of the QPG in Eq. (10). Table III summarises the outcome. The improvement is striking. We obtain fidelities of 99%

with the actual input state. One example of such a state is shown in Fig. 6. The decrease in fidelity from 5 to 7 dimensions is almost negligible and even without filtering, the values are still very high. This shows the power of proper detector calibration for state tomogra-

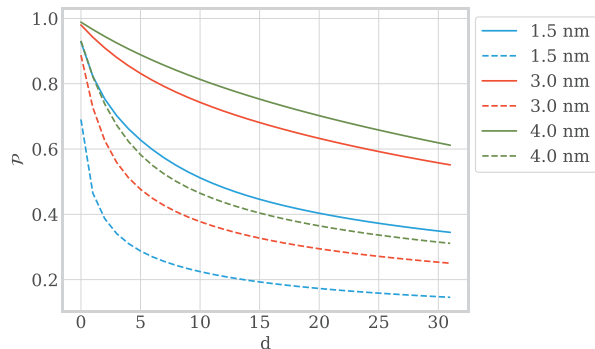


FIG. 5. Purity of QPG operation with respect to dimension. Solid lines are for a numerically modelled QPG as demonstrated in this paper. Each trace is labelled with the amplitude FWHM of the Gaussian function of the pump field. Dashed lines correspond to a numerically modelled QPG with the scheme presented in [11]. The purity is defined as $\mathcal{P} = 1/\sum_k \lambda_k^2$. For these calculations, we assumed a Gaussian phase-matching distribution and an interaction length of 1 cm.

phy. The outstanding fidelities suggest that the state tomography with QPG can be scaled up to higher dimensions. However performing a complete detector tomography for higher dimensions, with the current experimental configuration, would require an impractically long measurement time. This is primarily a technical challenge to decrease the switching time of the SLMs and increase the count rates per second. From the numeric point of view, detector tomography becomes time consuming very quickly. Here, one could switch to pattern tomography [19], which circumvents this tedious step by fitting the detector response pattern directly. We tested this approach as well and obtained similar fidelities as shown in Table III.

CONCLUSION

In conclusion we have shown that the QPG is capable of performing mode sensitive operations on arbitrary modes. We demonstrated good fidelities between the reconstructed measurement operators and an ideal QPG. We have further shown that using these operators for state tomography drastically improves the fidelities of the reconstructed states to about 99%. This shows the potential of this device for high-dimensional quantum information science with temporal modes.

FUNDING INFORMATION

This research has received funding from the Gottfried Wilhelm Leibniz-Preis and from the European Unions Horizon 2020 research and innovation programme under grant agreement No 665148.

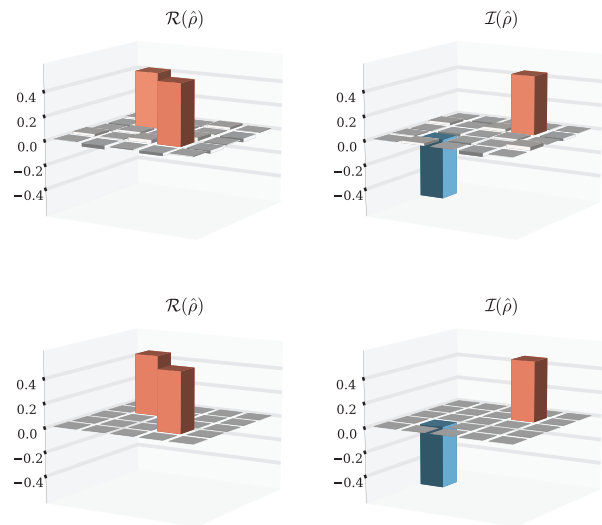


FIG. 6. Density matrix of the state $|1\rangle - i|3\rangle$ in Hermite-Gaussian basis in 5 dimensional space. Top: experimentally reconstructed with 99% fidelity. Bottom: theoretical.

ACKNOWLEDGMENTS

The authors would like to thank Nicolas Treps, Jonathan Roslund, John Donohue, Saleh Rahimi-Keshari and Dileep V. Reddy for helpful discussions.

* vahid.ansari@uni-paderborn.de

- [1] B. Brecht, D. V. Reddy, C. Silberhorn, and M. G. Raymer, *Physical Review X* **5**, 041017 (2015).
- [2] T. C. Ralph, I. Söllner, S. Mahmoodian, A. G. White, and P. Lodahl, *Physical Review Letters* **114**, 173603 (2015).
- [3] J. Nunn, I. A. Walmsley, M. G. Raymer, K. Surmacz, F. C. Waldermann, Z. Wang, and D. Jaksch, *Physical Review A* **75**, 011401 (2007).
- [4] Z. Zheng, O. Mishina, N. Treps, and C. Fabre, *Physical Review A* **91**, 031802 (2015).
- [5] K. E. Dorfman, F. Schlawin, and S. Mukamel, *The Journal of Physical Chemistry Letters* **5**, 2843 (2014).
- [6] B. Brecht, A. Eckstein, A. Christ, H. Suche, and C. Silberhorn, *New Journal of Physics* **13**, 065029 (2011).
- [7] A. Eckstein, B. Brecht, and C. Silberhorn, *Optics Express* **19**, 13770 (2011).
- [8] D. V. Reddy, M. G. Raymer, C. J. McKinstrie, L. Mejling, and K. Rottwitz, *Optics Express* **21**, 13840 (2013).
- [9] B. Brecht, A. Eckstein, R. Ricken, V. Quiring, H. Suche, L. Sansoni, and C. Silberhorn, *Physical Review A* **90**, 030302 (2014).
- [10] A. S. Kowligy, P. Manurkar, N. V. Corzo, V. G. Velez, M. Silver, R. P. Scott, S. J. B. Yoo, P. Kumar, G. S. Kanter, and Y.-P. Huang, *Optics Express* **22**, 27942 (2014).

- [11] P. Manurkar, N. Jain, M. Silver, Y.-P. Huang, C. Langrock, M. M. Fejer, P. Kumar, and G. S. Kanter, *Optica* **3**, 1300 (2016).
- [12] A. Christ, B. Brecht, W. Maurer, and C. Silberhorn, *New Journal of Physics* **15**, 053038 (2013).
- [13] N. Quesada and J. E. Sipe, *Physical Review Letters* **114**, 093903 (2015).
- [14] N. Quesada and J. E. Sipe, *Optics Letters* **41**, 364 (2016).
- [15] F. Krumm, J. Sperling, and W. Vogel, *Physical Review A* **93**, 063843 (2016).
- [16] P. M. Leung, W. J. Munro, K. Nemoto, and T. C. Ralph, *Physical Review A* **79**, 042307 (2009).
- [17] D. V. Reddy, M. G. Raymer, and C. J. McKinstrie, *Physical Review A* **91**, 012323 (2015).
- [18] Bandyopadhyay, Boykin, Roychowdhury, and Vatan, *Algorithmica* **34**, 512 (2002).
- [19] J. Rehacek, D. Mogilevtsev, and Z. Hradil, *Physical Review Letters* **105**, 010402 (2010).